SUPPLEMENTARY FIGURE 1

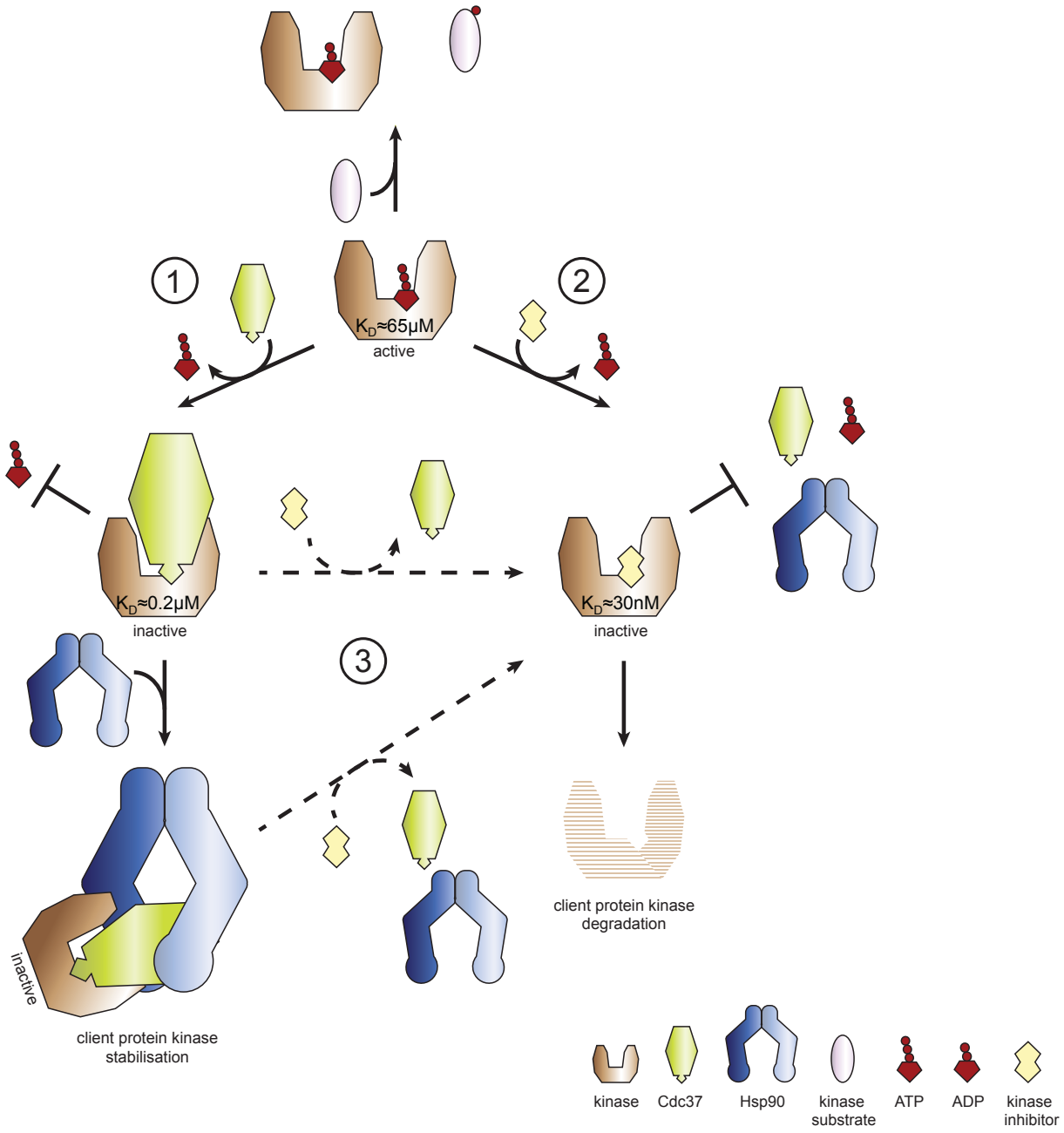

Supplementary Figure 1 – The Hsp90 co-chaperone Cdc37 controls the catalytic activity of client protein kinases and is antagonised by ATP-competitive kinase inhibitors

Kinases phosphorylate downstream targets in presence of ATP. ATP binding is antagonised by Cdc37 binding **(1)** to the client protein kinase. Thus, in complex with Cdc37 – and also with Cdc37 and Hsp90 – the kinase is kept in an inactive state, meaning that the Hsp90-Cdc37 system directly controls client protein kinase activity. ATP-competitive kinase inhibitors that bind kinases much tighter than ATP and that are used as anti-cancer drugs appear to have a dual mode of action **(2)**: They not only prevent ATP binding to the kinase, but also Cdc37 and Hsp90 binding. Since the interaction with the Hsp90 system is essential for the cellular stability of client protein kinases, this ultimately leads to kinase destabilisation and degradation. To a certain extent, ATP-competitive kinase inhibitors are able to break existing Cdc37-kinase and Hsp90-Cdc37-kinase complexes (dashed lines, **3**). Chaperone deprivation and client kinase degradation might constitute a significant component of the pharmacological effect of ATP-competitive kinase inhibitors on tumour cells.

SUPPLEMENTARY FIGURE 2

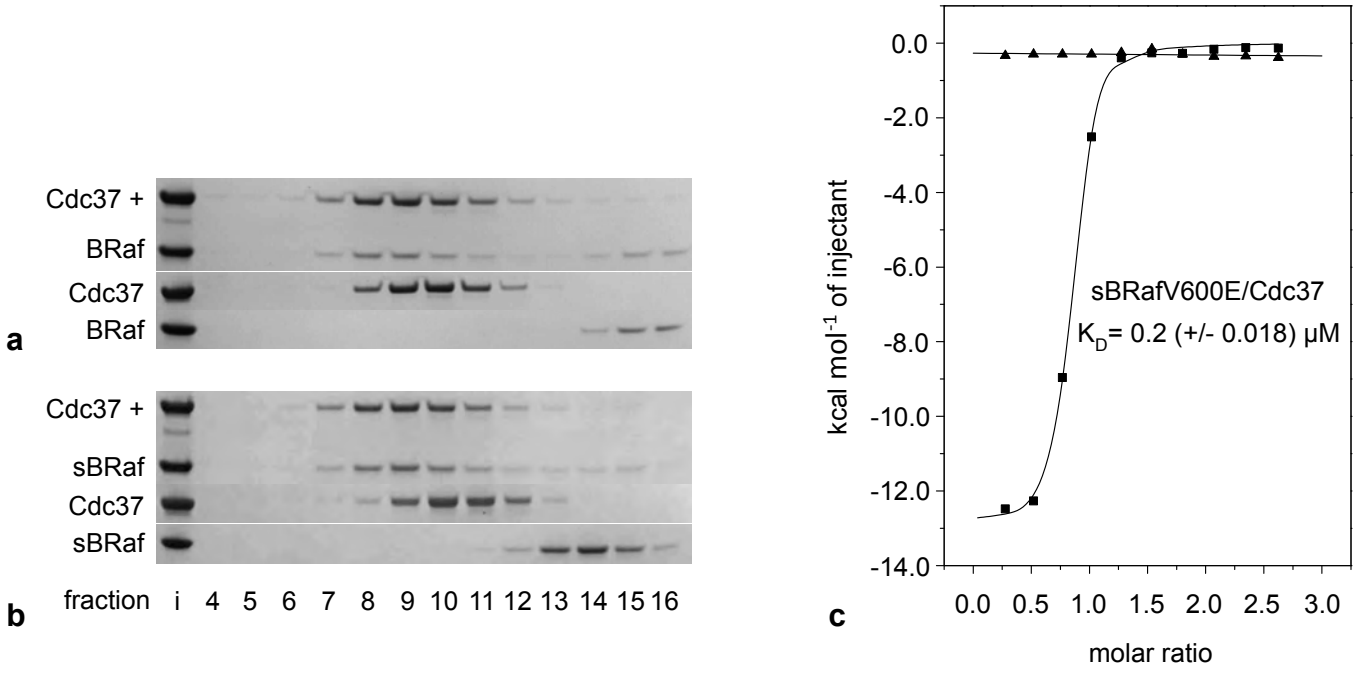

Supplementary Figure 2 – BRaf catalytic domain association with Cdc37

a. Coomassie stained SDS-PAGE gels of fractions eluting from a Superose 6 gel filtration column – 'i': input; bottom: BRaf kinase domain only (expressed in *Sf9* insect cells); middle: Cdc37 only; top: BRaf + Cdc37. Co-elution of BRaf and Cdc37 and the shift of both proteins to elution in earlier-running fractions show formation of a stable BRaf-Cdc37 complex.

b. As **a**, but with the solubilised BRaf kinase domain (expressed in *E. coli*).

c. Isothermal titration calorimetry trace for injection of sBRafV600E into Cdc37 (■) or buffer (▲). sBRafV600E binds Cdc37 with a K_D of 0.2 (+/- 0.018) µM at a 1:1 stoichiometry.

SUPPLEMENTARY FIGURE 3

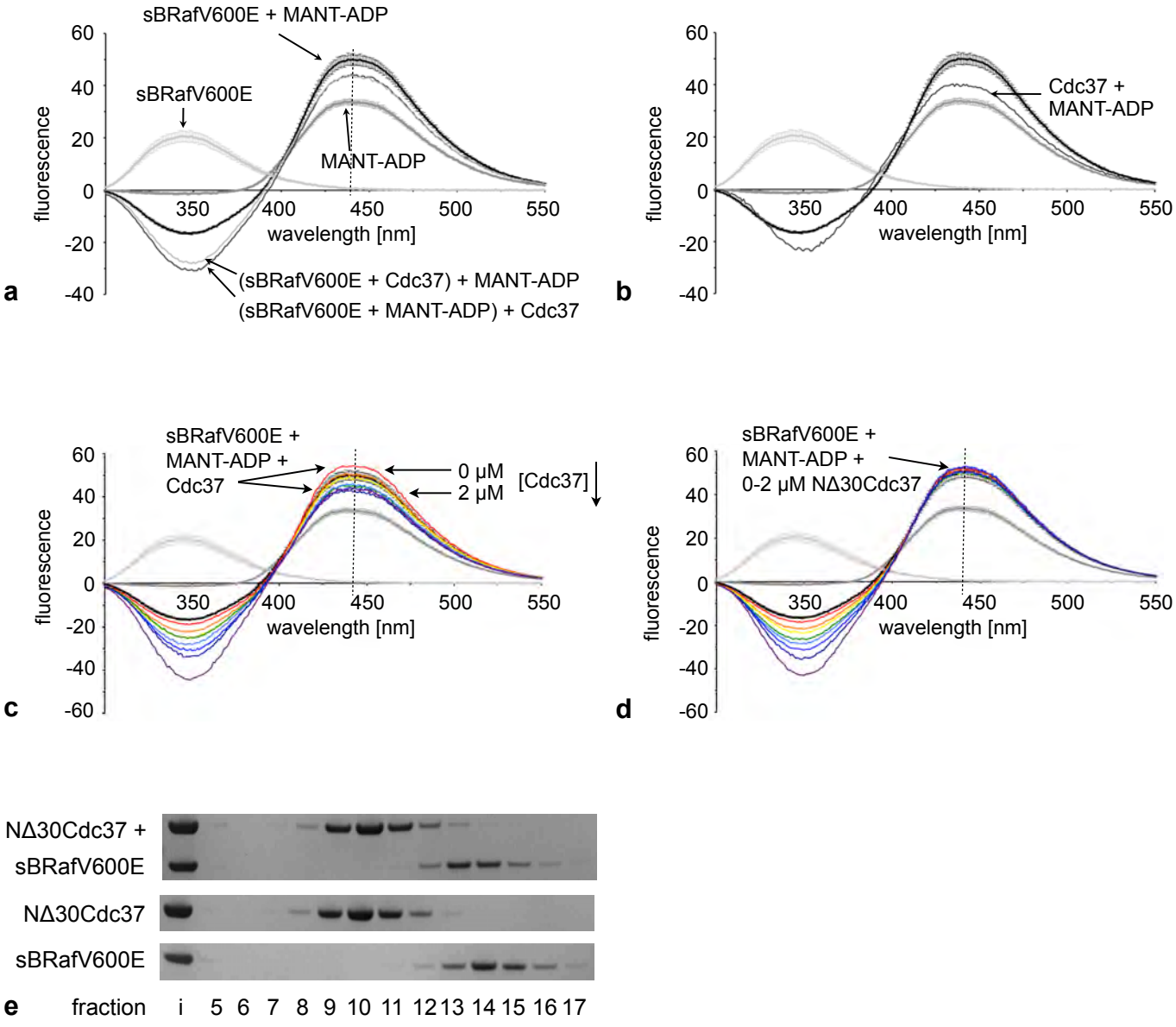

Supplementary Figure 3 – Cdc37 antagonises MANT-ADP binding to sBRafV600E

a. Addition of 1µM Cdc37 to a pre-incubated mixture of 1µM sBRafV600E and 120µM MANT-ADP decreases the fluorescence enhancement of sBRafV600E●MANT-ADP at 440nm to the same extent as addition of MANT-ADP to a pre-formed complex of sBRafV600E and Cdc37. As reference, fluorescence emission spectra for MANT-ADP and sBRafV600E alone and incubated together are shown. Standard deviations of at least three independent experiments are indicated.

b. Fluorescence emission spectrum for Cdc37 (2µM) incubated with MANT-ADP (120µM). Cdc37 does not decrease the fluorescence of free MANT-ADP, nor does the BRaf binding impaired mutant NΔ30Cdc37 (data not shown). Reference spectra as in **a**.

c. Incubation of sBRafV600E●MANT-ADP with increasing concentrations of Cdc37 (0-2μM) progressively decreases the fluorescence enhancement at 440nm in a dose dependent fashion. The spectra are coloured according to the rainbow (0μM Cdc37: red, 2 μM Cdc37: violet). Reference spectra as in **a**.

d. As **c**. The BRaf binding impaired mutant NΔ30Cdc37 does not decrease the fluorescence enhancement of sBRafV600E●MANT-ADP at 440nm at any of the concentrations tested.

e. Coomassie stained SDS-PAGE gels of fractions eluting from a Superose 6 gel filtration column – 'i': input; bottom: sBRafV600E kinase domain only; middle: NΔ30Cdc37 only; top: sBRafV600E + NΔ30Cdc37. In contrast to sBRafV600E + Cdc37 (**Fig. 1b**), sBRafV600E + NΔ30Cdc37 do not form a complex.

SUPPLEMENTARY FIGURE 4

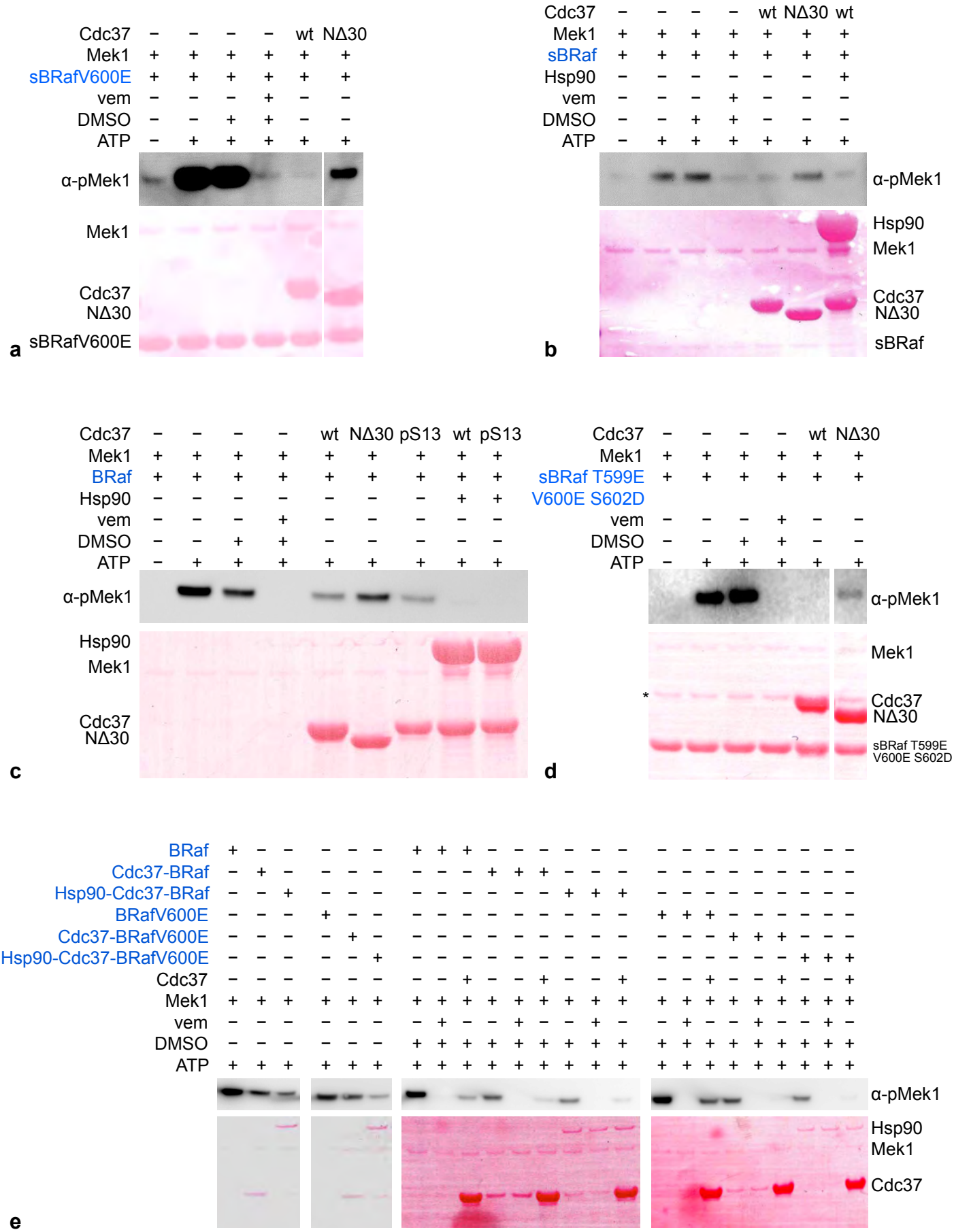

Supplementary Figure 4 – Cdc37 inhibits the kinase activities of sBRafV600E, sBRaf, sBRaf T599E V600E S602D, BRafV600E and BRaf

a. Kinase activity of *E. coli* expressed sBRafV600E visualised by western blotting of its downstream substrate Mek1, using a phospho-Mek1 antibody. Ponceau stained total Mek1 serves as loading control. Whereas no activity could be detected for *E. coli* expressed sBRaf under similar conditions (data not shown), the activating oncogenic V600E mutation confers measurable activity to sBRaf. sBRafV600E phosphorylation of Mek1 is not affected in the DMSO control, but effectively inhibited by vemurafenib and equimolar amounts of full length Cdc37 (10μM). A Cdc37 truncation mutant impaired in kinase binding is substantially less effective in inhibiting Mek1 phosphorylation (see also **Fig. 2e**).

b. Cdc37 (5μM) inhibits the kinase activity of sBRaf (0.38μM) expressed in *Sf9* insect cells, showing that it interacts similarly with both wild-type BRaf and the oncogenic V600E mutant. sBRaf is also inactive in presence of Cdc37 and Hsp90. For further details see **a**.

c. Cdc37 (5μM) inhibits the kinase activity of *Sf9* insect cell expressed BRaf (75nM), proving that the co-chaperone interacts similarly with solubilized and wild-type forms of BRaf. The 16 solubilizing surface mutations in sBRaf and sBrafV600E do not affect the interaction with Cdc37. Phosphorylation of Cdc37 on Ser13 by CKII does not influence its ability to inhibit Mek1 phosphorylation, neither alone nor in complex with Hsp90. For further details see **a**.

d. Equimolar amounts of Cdc37 (10μM) inhibit the kinase activity of constitutively active sBRaf T599E V600E S602D[31]. * Impurity of sBRaf T599E V600E S602D preparation. For further details see **a**.

e. BRaf or BRafV600E (75nM) purified from *Sf9* insect cells show less activity in Mek1 phosphorylation when co-purified with Cdc37 or Cdc37-*Sf9* Hsp90 (2 left panels). The residual activities detected for the Cdc37 and Cdc37-*Sf9* Hsp90 complexes can be inhibited with vemurafenib and additional Cdc37 (2 right panels). The residual activities are most probably due to free BRaf or BRafV600E that dissociate from the complexes at a concentration far below the K_D (200nM).

SUPPLEMENTARY FIGURE 5

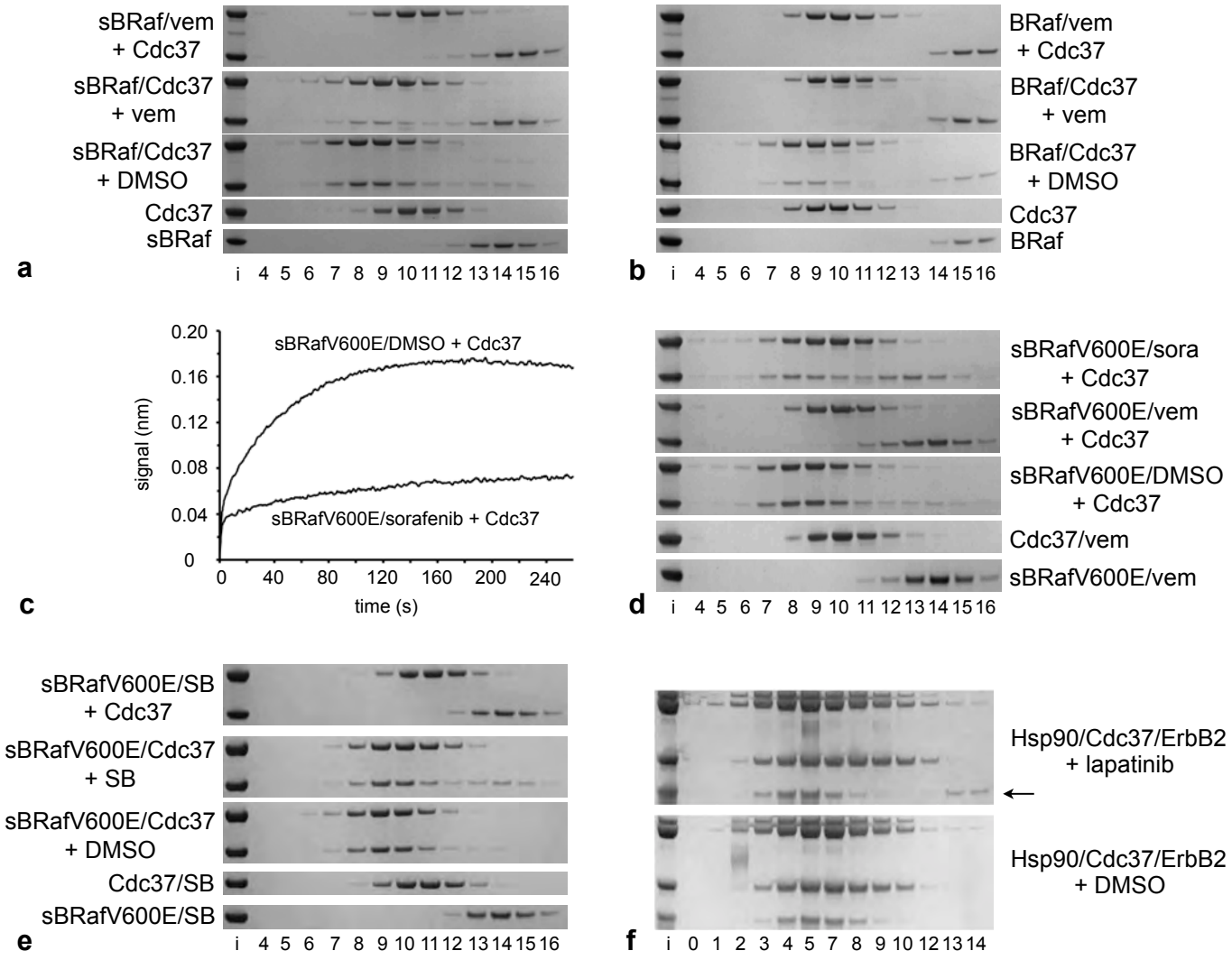

Supplementary Figure 5 – ATP-competitive inhibitors antagonise Cdc37 binding to BRaf

a. Coomassie stained SDS-PAGE gels showing the gel filtration elution profiles of (top to bottom): Cdc37 incubated with a pre-formed sBRaf-vemurafenib complex; a pre-formed sBRaf-Cdc37 complex incubated with vemurafenib; a pre-formed sBRaf-Cdc37 complex incubated with DMSO; Cdc37 only; sBRaf only. As with sBRafV600E, vemurafenib prevents sBRaf recruitment to Cdc37. The disassembly of pre-formed Cdc37-sBRaf is more efficient than of Cdc37-sBRafV600E, possibly reflecting a tighter binding of the drug to BRaf than to BrafV600E (in absence of ATP), similar to the tighter binding of ATP to BRaf than to BRafV600E[28].

b. As **a**. Vemurafenib prevents recruitment of BRaf to Cdc37 and displaces BRaf from a Cdc37-BRaf complex.

c. Octet Biosensor association curve for Cdc37 binding to sBRafV600E immobilised on the sensor tip via its N-terminal His_6-tag. Binding is substantially inhibited in the presence of sorafenib.

d. Coomassie stained SDS-PAGE gels showing Superose 6 elution profiles (top to bottom): Cdc37 incubated with a pre-formed sBRafV600E-sorafenib complex; Cdc37 incubated with a pre-formed sBRafV600E-vemurafenib complex; sBRafV600E/DMSO incubated with Cdc37; Cdc37 incubated with vemurafenib; sBRafV600E incubated with vemurafenib. Sorafenib is slightly less efficient than vemurafenib in preventing recruitment of Cdc37 to sBRafV600E.

e. Coomassie stained SDS-PAGE gels showing the gel filtration elution profiles of (top to bottom): Cdc37 incubated with a pre-formed sBRafV600E-SB-590885 complex; a pre-formed sBRafV600E-Cdc37 complex incubated with SB-590885; a pre-formed sBRafV600E-Cdc37 complex incubated with DMSO; Cdc37 incubated with SB-590885; sBRafV600E incubated with SB-590885. SB-590885 is as efficient as vemurafenib in preventing recruitment of Cdc37 to sBRafV600E.

f. Silver stained SDS-PAGE gels showing the gel filtration elution profiles of Hsp90/Cdc37/ErbB2 complexes purified from *Sf9* cells and incubated with lapatinib (top) or DMSO (bottom). The *in vivo* assembled Hsp90/Cdc37/ErbB2 complex is destabilised by lapatinib, releasing some free ErbB2 kinase domain.

SUPPLEMENTARY FIGURE 6

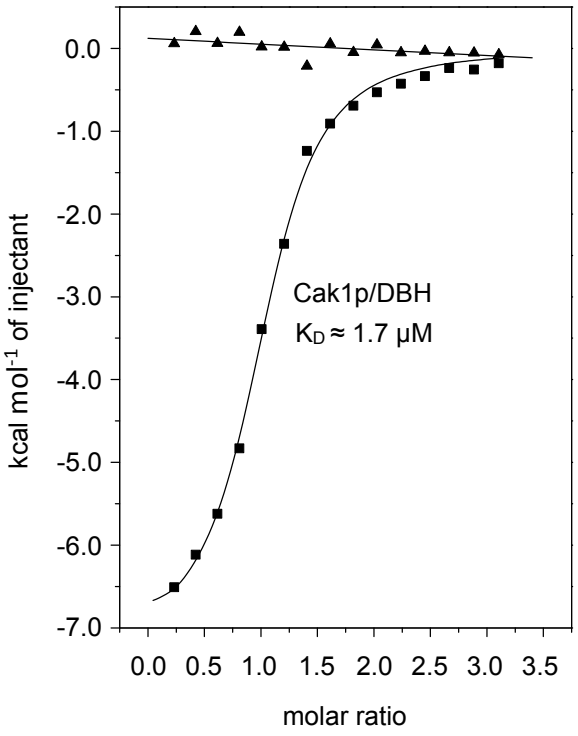

Supplementary Figure 6 – Debromohymenialdisine binds to Cak1p

Isothermal titration calorimetry trace for injection of Cak1p into debromohymenialdisine (■) or buffer (▲). The low-specificity protein kinase inhibitor debromohymenialdisine binds Cak1p with a K_D of ~1.7μM at a 1:1 stoichiometry.

SUPPLEMENTARY FIGURE 7

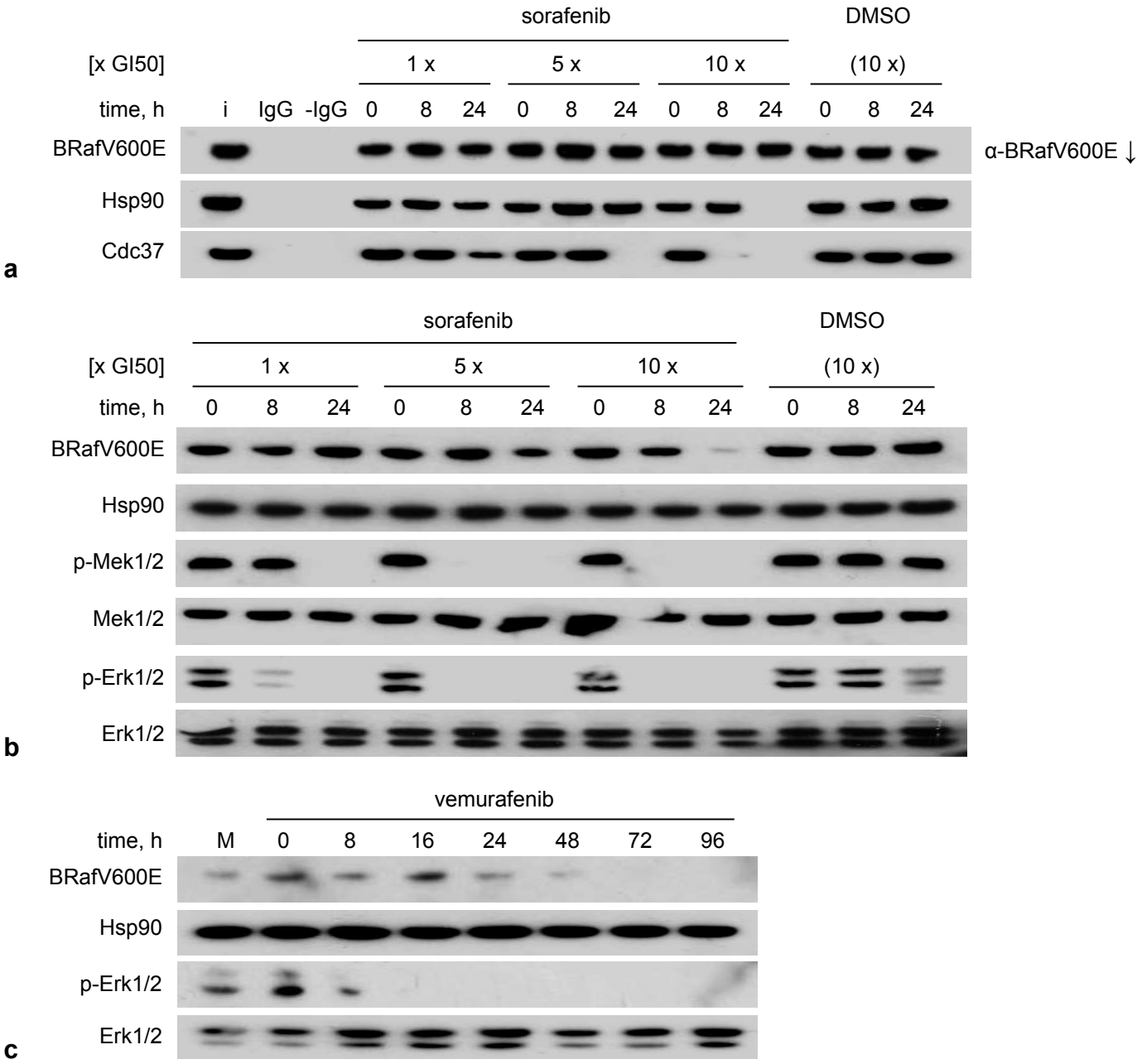

Supplementary Figure 7 – Prevention of BRafV600E association with Cdc37-Hsp90 in intact cells by ATP-competitive kinase inhibitors

a. Western blots of BRafV600E immunoprecipitated from HT29 colon cancer cells incubated in the presence of different concentrations of sorafenib (expressed as multiples of GI50 – the concentration that gives 50% growth inhibition) for different periods of time. The GI50 for 96 hours continuous exposure to sorafenib was determined as 3.7μM. Controls are 'i': cell lysate input; IgG: α-BRafV600E IgG but no protein; -IgG: protein but no α-BRafV600E IgG. DMSO controls are at [DMSO] used in the 10x GI50 incubation with sorafenib. Cdc37 and Hsp90 are progressively depleted in co-immunoprecipitates at higher drug exposure.

b. Western blots of cell lysates from HT29 cells incubated in the presence of different concentrations of sorafenib for different periods of time. Signalling downstream of BRafV600E, measured by Mek and Erk phosphorylation, is decreased by sorafenib levels that deplete Cdc37 and Hsp90 from BRafV600E co-immunoprecipitates. High levels of exposure to the drug decrease cellular BRafV600E levels.

c. Western blots of cell lysates from HT29 cells incubated with 1x GI50 vemurafenib (0.46μM) for different periods of time. 'M': 96 hours DMSO vehicle exposure. High levels of exposure to the drug decrease cellular BRafV600E but not Erk levels. All experiments were performed in triplicate, representative results are shown.

SUPPLEMENTARY FIGURE 8

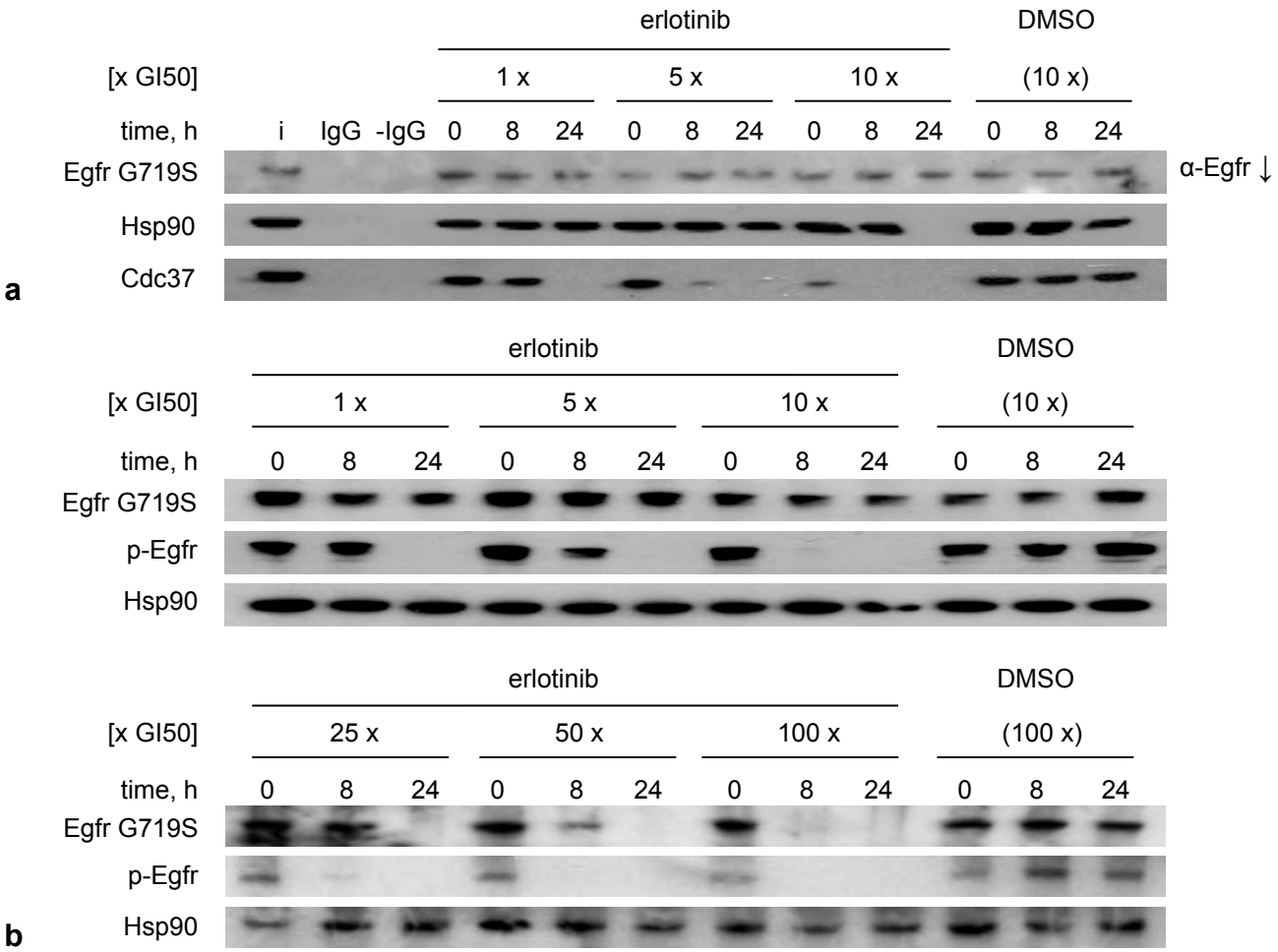

Supplementary Figure 8 – Prevention of mutant Egfr association with Cdc37-Hsp90 in intact cells with erlotinib

a. Western blots of Egfr G719S immunoprecipitated from SW48 colon adenocarcinoma cells incubated in the presence of different concentrations of erlotinib (expressed as multiples of GI50 – the concentration that gives 50% growth inhibition) for different periods of time. The GI50 for 96 hours continuous exposure to erlotinib was determined as 1.25μM. Controls are 'i': cell lysate input; IgG: α-Egfr IgG but no protein; -IgG: protein but no α-Egfr IgG. DMSO controls are at [DMSO] used in the 10x GI50 incubation with erlotinib. Cdc37 and Hsp90 are progressively depleted in co-immunoprecipitates at higher drug exposure.

b. Western blots of cell lysates from SW48 cells incubated in the presence of different concentrations of erlotinib for different periods of time. Egfr G719S kinase activity measured by auto-phosphorylation is decreased by erlotinib levels that deplete Cdc37 and Hsp90 from Egfr G719S co-immunoprecipitates. High levels of exposure to the drug are accompanied by a decrease in cellular Egfr G719S levels. All experiments were performed in triplicate, representative results are shown.

SUPPLEMENTARY FIGURE 9

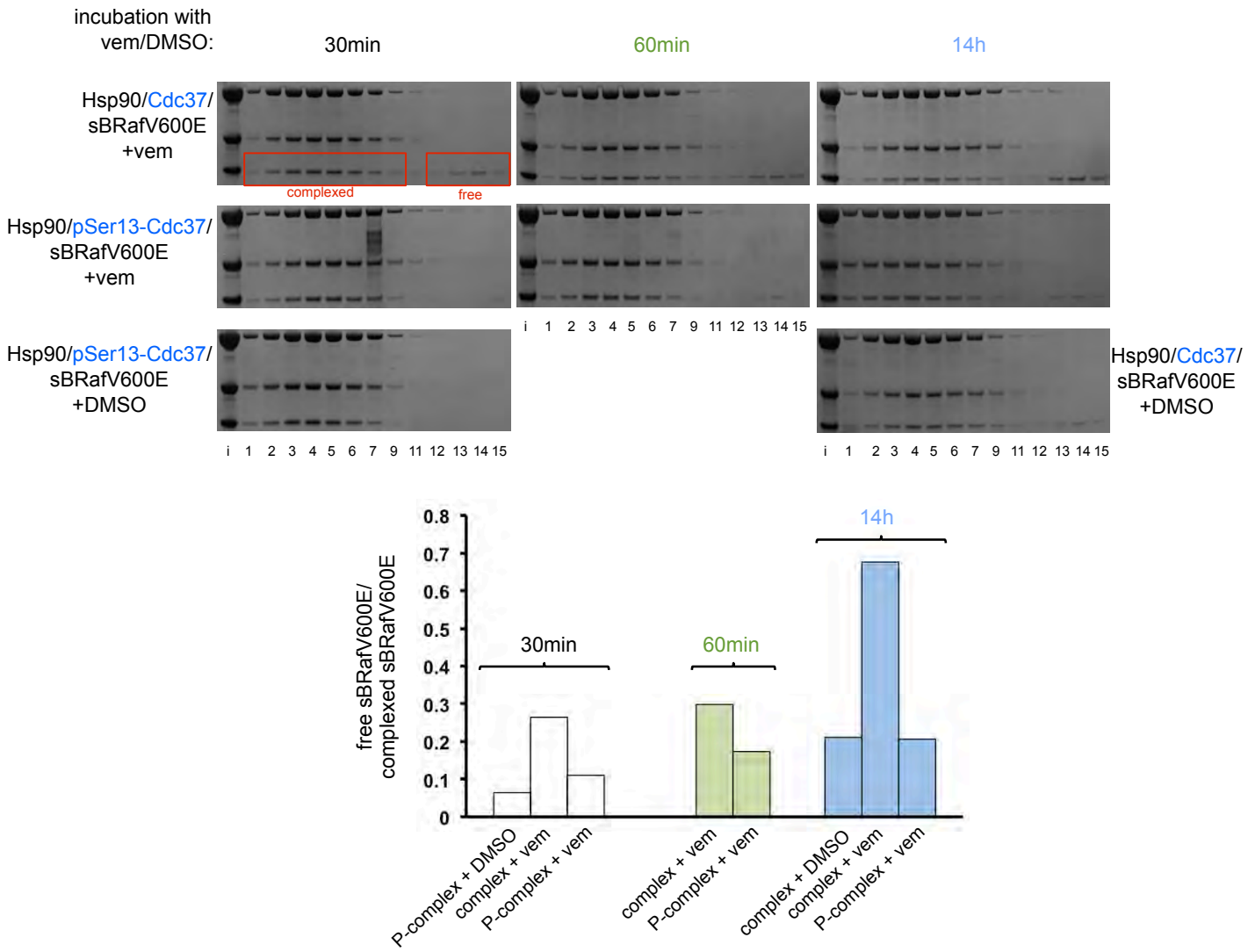

Supplementary Figure 9 – Ser13 phosphorylation of Cdc37 stabilises Hsp90/Cdc37/sBRafV600E complex to disruption by vemurafenib

In vitro assembled Hsp90/Cdc37/sBRafV600E or Hsp90/pSer13-Cdc37/sBRafV600E were incubated with vemurafenib or DMSO for 30min, 60min or 14h. The density of free sBRafV600E (fractions 12-15) and complexed sBRafV600E (fractions 1-9) was determined using AIDA and presented in a graph - 'complex': Hsp90/Cdc37/sBRafV600E; 'P-complex': Hsp90/pSer13-Cdc37/sBRafV600E. At all time points, Hsp90/pSer13-Cdc37/sBRafV600E is more stable against dissociation by vemurafenib than Hsp90/Cdc37/sBRafV600E.

SUPPLEMENTARY FIGURE 10

Figure 1a, left

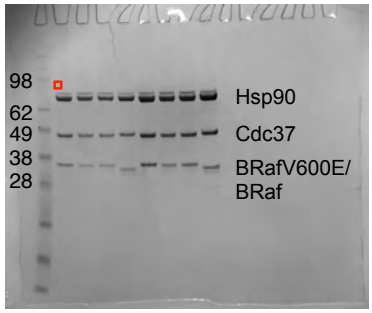

Figure 1a, middle
elution from Strep-Tactin

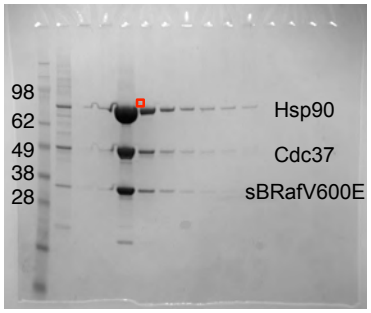

Figure 1a, right
elution from HiTrap SP

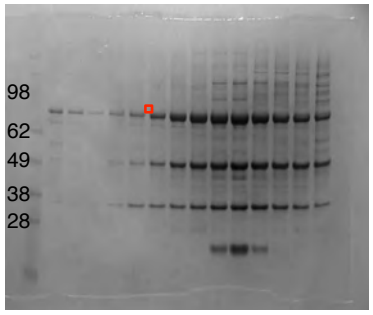

Figure 1b, row 1

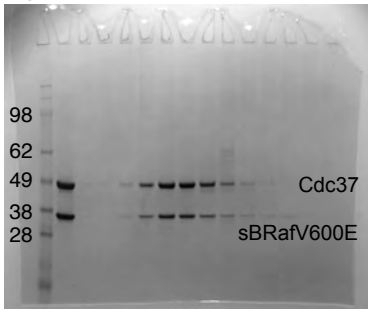

Figure 1b, row 2

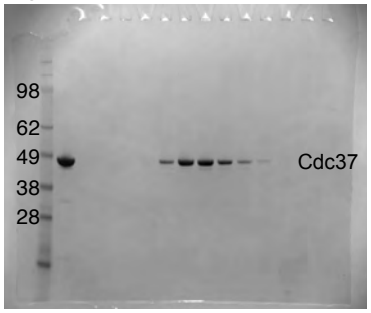

Figure 1b, row 3

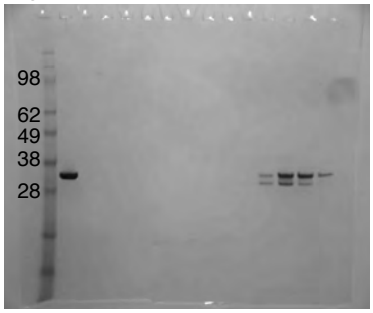

Figure 1c, row 1

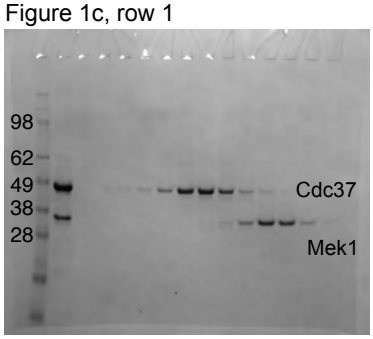

Figure 1c, row 2

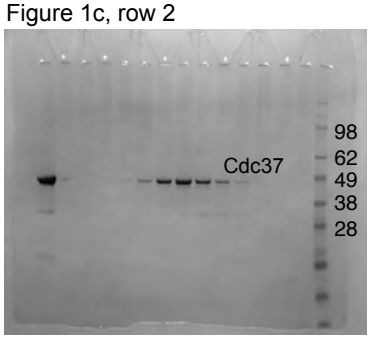

Figure 1c, row 3

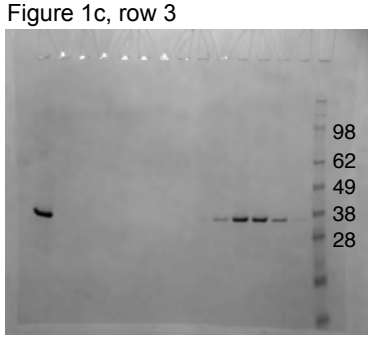

Figure 1d, row 1

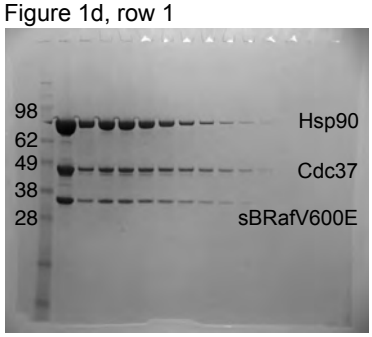

Figure 1d, row 2

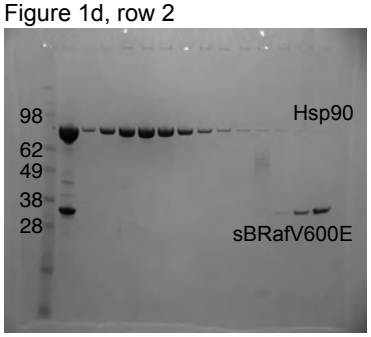

Figure 1d, row 3

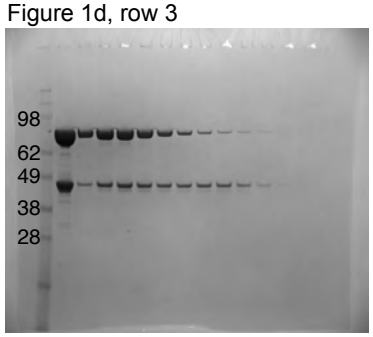

Figure 1d, row 4

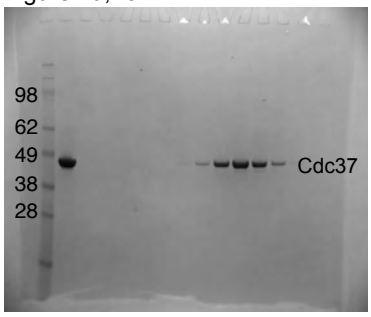

Figure 1d, row 5

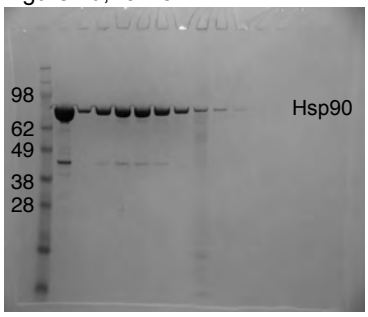

Supplementary Figure 10 – Uncropped Coomassie stained SDS-PAGE gels used for Figure 1

SUPPLEMENTARY FIGURE 11

Figure 2c, row 1

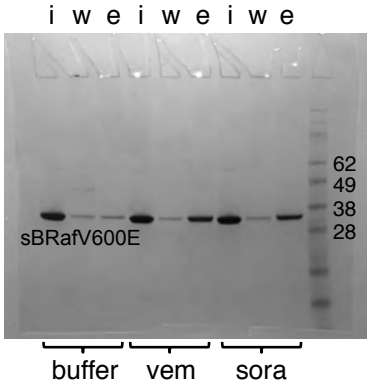

Figure 2c, row 2 left

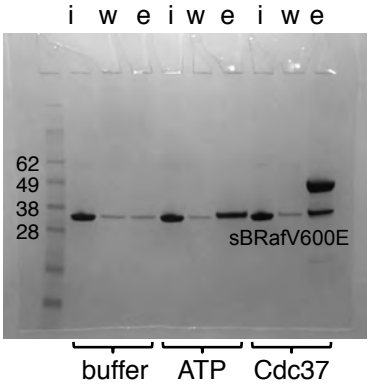

Figure 2c, row 2 right

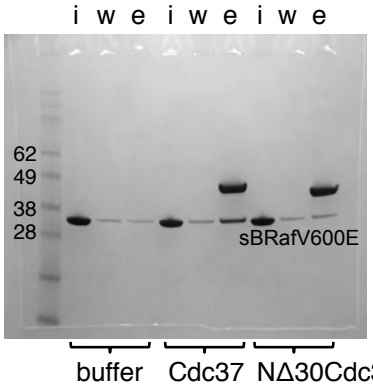

Figure 2d, left

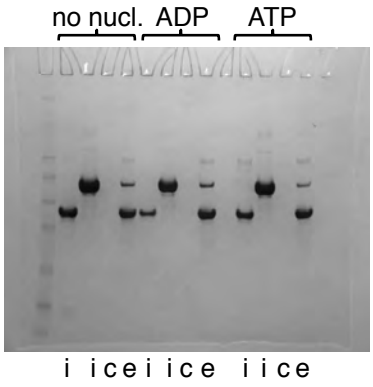

Figure 2d, right

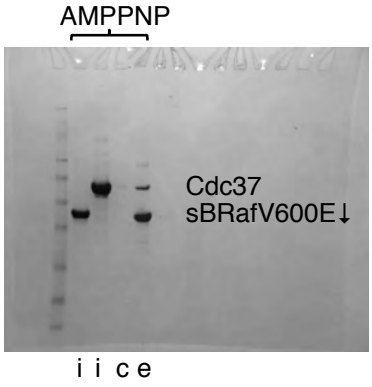

Figure 2e

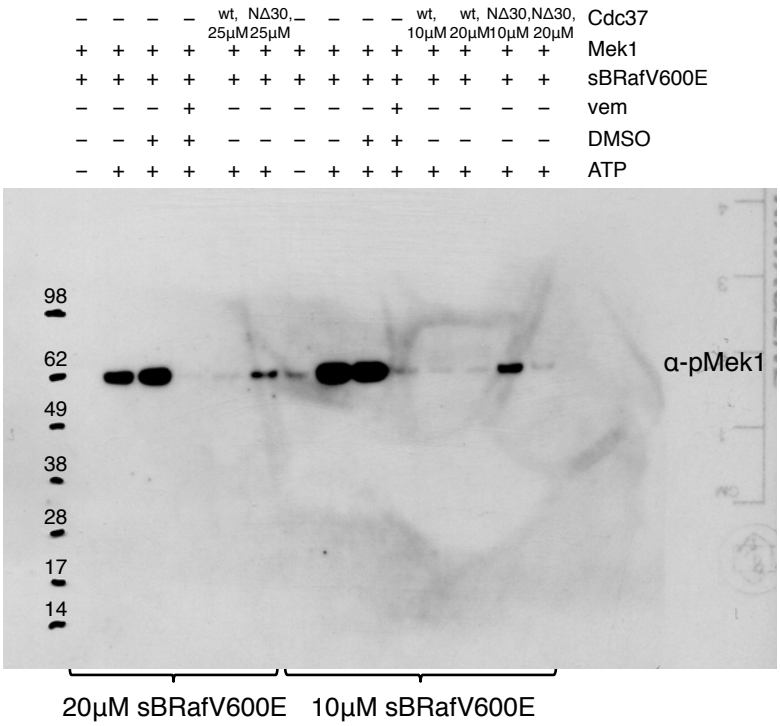

Supplementary Figure 11 – Uncropped Coomassie stained SDS-PAGE gels and western blots used for Figure 2

SUPPLEMENTARY FIGURE 12

Figure 3b, row 1

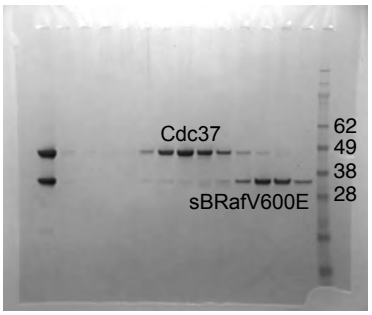

Figure 3b, row 2

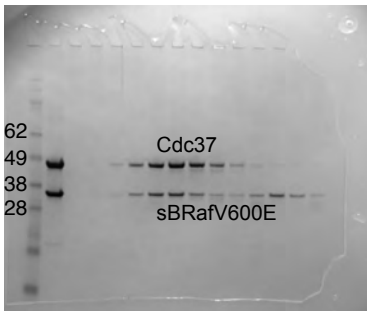

Figure 3b, row 3

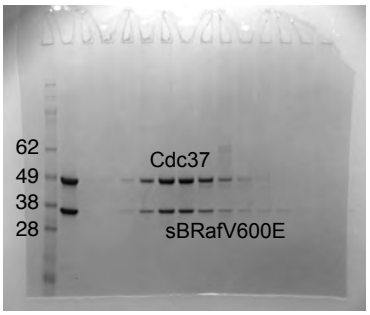

Figure 3b, row 4

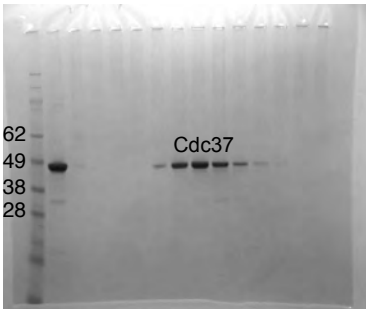

Figure 3b, row 5

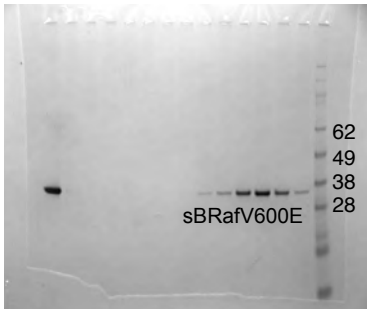

Figure 3c, row 1

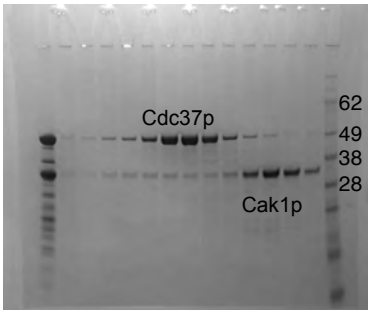

Figure 3c, row 2

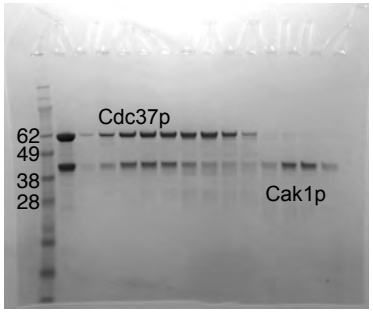

Figure 3c, row 3

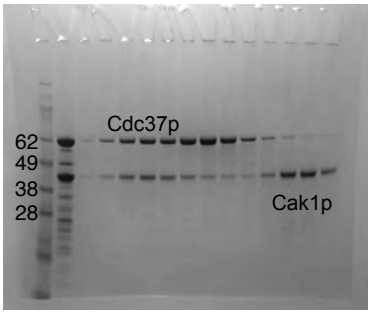

Figure 3c, row 4

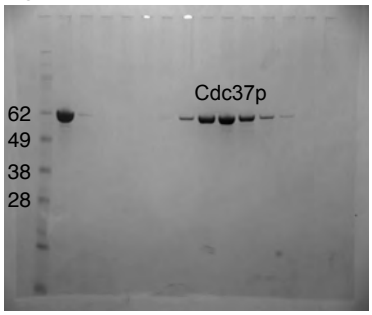

Figure 3c, row 5

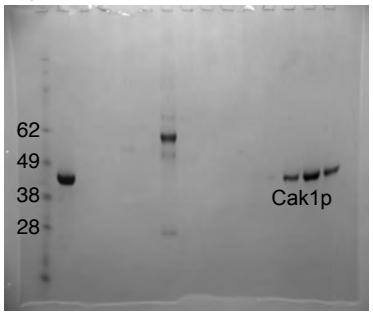

Figure 3d, row 1

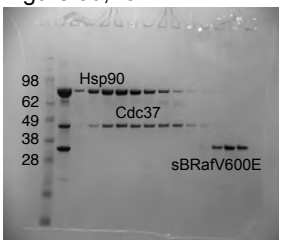

Figure 3d, row 2

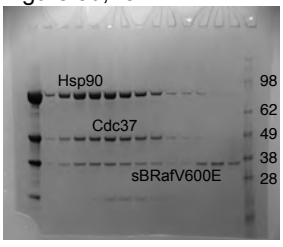

Figure 3d, row 3

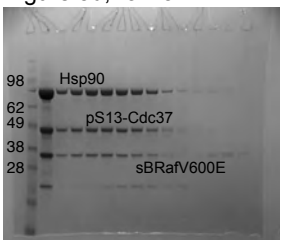

Figure 3d, row 4

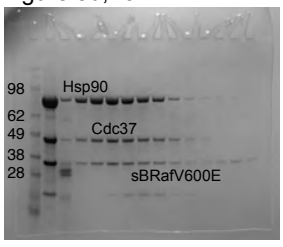

Supplementary Figure 12 – Uncropped Coomassie stained SDS-PAGE gels used for Figure 3

SUPPLEMENTARY FIGURE 13

Figure 4a, row 1, BRafV600E

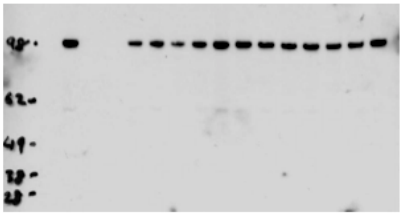

Figure 4a, row 2, Hsp90

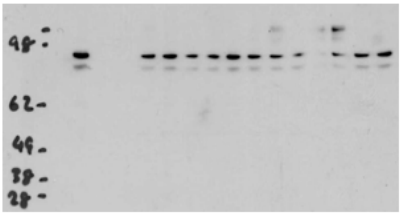

Figure 4a, row 3, Cdc37

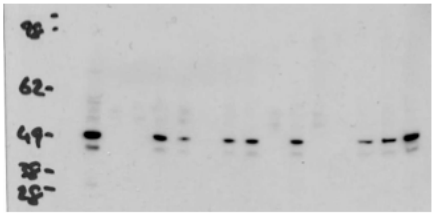

Figure 4b, row 1, BRafV600E

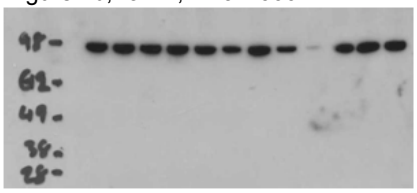

Figure 4b, row 2, Hsp90

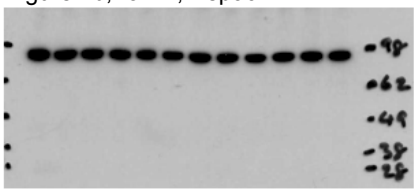

Figure 4b, row 3, p-Mek1/2

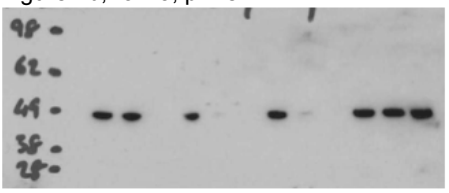

Figure 4b, row 4, Mek1/2

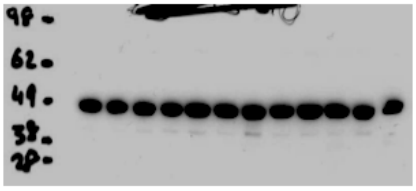

Figure 4b, row 5, p-Erk1/2

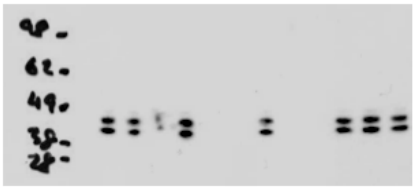

Figure 4b, row 6, Erk1/2

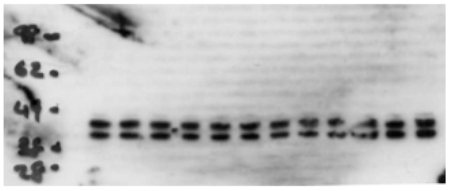

Figure 4c, rows 1 and 2, ErbB2 and Hsp90

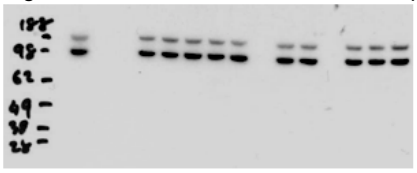

Figure 4c, row 3, Cdc37

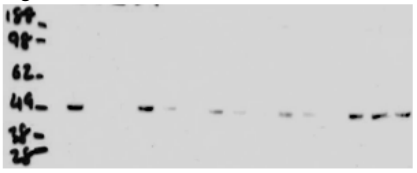

Figure 4d, row 1, ErbB2

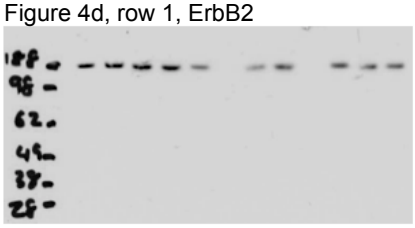

Figure 4d, row 2, p-ErbB2

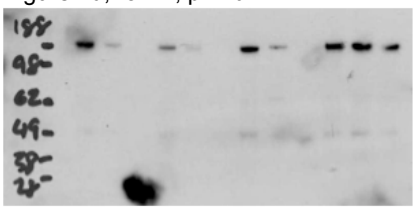

Figure 4d, row 3, Hsp90 (highest band)

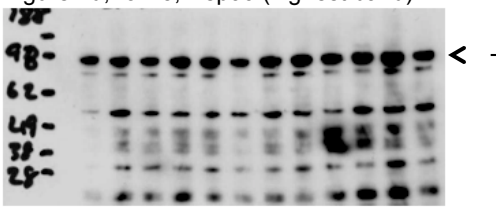

Figure 4e, row 1, BRafV600E (soluble)

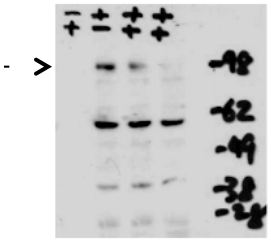

Figure 4e, rows 2 and 3, Hsp90 and GAPDH

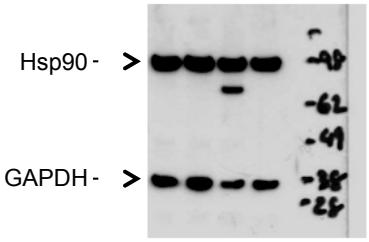

Figure 4e, right, BRafV600E (insoluble)

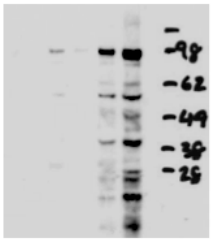

Supplementary Figure 13 – Uncropped western blots used for Figure 4

SUPPLEMENTARY FIGURE 14

Figure 5b, row 1,
BRafV600E

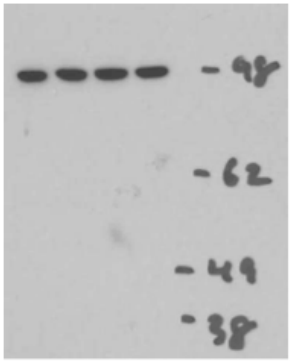

Figure 5b, row 2,
Cdc37

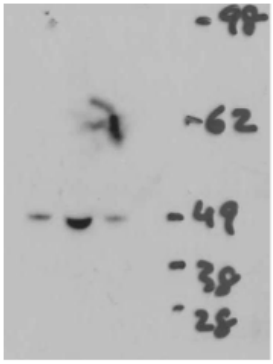

Figure 5b, row 3,
GAPDH (developed digitally)

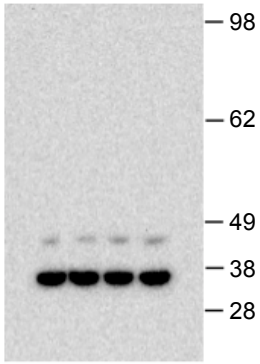

Supplementary Figure 14 – Uncropped western blots used for Figure 5